Chinese Chemical Letters 34 (2023) 107476

Contents lists available at ScienceDirect

Chinese Chemical Letters

journal homepage: www.elsevier.com/locate/cclet

# Screening promising TM-doped $CeO_2$ monolayer for formaldehyde sensor with high sensitivity and selectivity

Zhouhao Zhu[a,b], Hengcong Tao[a,c], Jingbin Fu[a], Yingtang Zhou[d], Jian Guo[a,*], Chunyang Zhai[a,e,*]

[a] School of Petrochemical Engineering & Environment, Zhejiang Ocean University, Zhoushan 316022, China
[b] School of Port and Transportation Engineering, Zhejiang Ocean University, Zhoushan 316022, China
[c] College of Chemical and Biological Engineering, Zhejiang University, Hangzhou 310058, China
[d] Key Laboratory of Key Technical Factors in Zhejiang Seafood Health Hazards, Zhejiang Ocean University, Zhoushan 316022, China
[e] School of Materials Science and Chemical Engineering, Ningbo University, Ningbo 315211, China

ARTICLE INFO

*Article history:*
Received 28 January 2022
Revised 26 February 2022
Accepted 26 April 2022
Available online 1 May 2022

*Keywords:*
Cerium oxide
Density functional theory
Formaldehyde
Metal doping

ABSTRACT

Developing convenient, fast-response and high-performance formaldehyde detection sensor is significant but challenging. Herein, two $CeO_2$ phases ($Fm\bar{3}m$ and $P4_2/mnm$), three facets ($CeO_2(100)$, $CeO_2(110)$ and $CeO_2(111)$) and three adsorption sites (top, bridge and hollow) are selected as substrate to interact with formaldehyde. Twenty-eight candidated transition metals (TM) are doped on $CeO_2$ surfaces to investigate the performance of detecting formaldehyde by density functional theory. It shows that (i) $CeO_2$ in a cubic fluorite structure with the space group $Fm\bar{3}m$ is suitable for formaldehyde adsorption compared with $P4_2/mnm$; (ii) TM-$CeO_2(100)$ (TM = Au, Hf, Nb, Ta, Zr) are considered as candidated materials to absorb formaldehyde ascribed to lower adsorption energies. The d-band center, partial density of states, charge density difference and electron localization function are employed to clarify the mechanism of TM-doped $CeO_2$ improving the performance of formaldehyde adsorption. It obviously displays that TM doped $CeO_2(100)$ changes the d orbit and rearranges electrons resulting in the superior ability to the adsorbed formaldehyde. This work provides theoretical guidance and experimental motivation for the development of novel formaldehyde sensor based on metal oxide semiconductor materials.



Formaldehyde (HCHO) is one kind of colorless poisonous volatile organic compounds (VOC) synthesized by the oxidation of methanol and widely used as an antiseptic, disinfectant and histologic fixative [1]. It is unavoidably released from artificial building decoration materials including coatings, paints, and resins [2]. Previous reports have shown that high-dose exposure increases the risk of acute poisoning and long-term exposure could lead to chronic poisoning or even cancer [3]. The International Agency for Research on Cancer (IARC) classified HCHO as a Group I carcinogen [4,5]. In addition, the World Health Organization (WHO) set the HCHO exposure limit as 0.08 ppm within 30 min [6]. Thus, the development of HCHO detection technology is great of urgent to daily life and industrial applications. The traditional techniques for the detection of HCHO include gas chromatography [7], electrochemistry [8] and spectrophotomete [9]. However, these detection techniques show many disadvantages, such as bulky equipment and complex detection steps [10]. Therefore, it is significance to develop convenient, fast-response and high-performance HCHO sensor.

Compared to bulky equipment, gas sensors based on metal oxide semiconductor (MOS) has recently attracted more attention owing to small size, low cost and facile operation [11–13], such as $CeO_2$, $SiO_2$, $Al_2O_3$ and $TiO_2$ [14]. Among them, $CeO_2$, featured by remarkable redox properties associated with facile conversion of $Ce^{4+}$ to $Ce^{3+}$ and strong interaction with metal, is widely investigated [15]. Many researchers have reported the excellent performance of $CeO_2$ in the detection of HCHO based on experiment results. Shahid *et al.* [16] prepared $CeO_2$ polyhedral nanostructures with highly exposed surface area. The result was shown that gas sensing response to HCHO is better than that of other target gasses at 150 ppm. Zhang *et al.* [17] provided ultra-thin $CeO_2$ nanosheets by a simple low-temperature hydrothermal method. It exhibited a fast response to 5–400 ppm HCHO vapor. D. S. Daniel *et al.* [18] proposed doping Zn ions into $CeO_2$ films and observed an obvious HCHO response in a lower detection (0.5 ppm) at 32 °C. The above works have proved that $CeO_2$ is a potential metal oxide

* Corresponding authors.
*E-mail addresses:* 025125@zjou.edu.cn (J. Guo), zhaichunyang@nbu.edu.cn (C. Zhai).

https://doi.org/10.1016/j.cclet.2022.04.074
1001-8417/

material for HCHO detection. However, these reports are obtained through prolonged trial and error, bulky equipment and complex experimental procedures. Therefore, it is of great significance to propose a simple method to improve the ability of $CeO_2$ to detect HCHO instead of the traditional experiment.

Density functional theory (DFT) [19] is a computational quantum mechanical modeling method used in physics, chemistry and materials science. It is widely used to explore materials for the detection of HCHO. For example, Deng *et al.* [20] studied the electronic properties of TM (TM = Ni, Pt, Ti, Pd) doped $MoS_2$ and the adsorption of HCHO on these monolayer 2D structures by DFT, shows that TM-doped can substantially improve the sensitivity towards HCHO. [21] Jing *et al.* [22] used the density functional theory with Hubbard U correction (DFT+U) to study the effect of Au doping $CeO_2$ on the adsorption HCHO. The authors believed that Au doping promoted the activation of surface oxygen and promoted the adsorption of HCHO. Hence, as a detection descriptor, adsorption can be employed to describe the performance of HCHO adsorption sensor. TM-doped $CeO_2$ to improve the adsorption capacity of HCHO by using DFT is considered to be an effective measure to improve the ability to detect HCHO. However, to the best of our knowledge, there is still a lack of relevant reports.

Inspired by above reports, two $CeO_2$ phases ($Fm\bar{3}m$ and $P4_2/mnm$), three facets ($CeO_2$(100), $CeO_2$(110) and $CeO_2$(111)) and three adsorption sites (top, bridge and hollow) are proposed to elucidate stability for HCHO adsorption. Afterwards, twenty-eight candidated TMs are doped on $CeO_2$ to simulate the adsorption performance of HCHO. It is found that $CeO_2$ in a cubic fluorite structure with the space group of $Fm\bar{3}m$ is favorable to HCHO adsorption compared with the $CeO_2$ ($P4_2/mnm$) base on DFT simulation. TM-$CeO_2$ (TM = Au, Hf, Nb, Ta, Zr) are considered as candidated materials for absorbing HCHO due to their lower adsorption energies than the other twenty-five TM-$CeO_2$. Finally, the d-band center, partial density of states and charge density difference are employed to explain the mechanism of improving the adsorption capacity of HCHO. The simulation solid date reveals that the improved performance of $CeO_2$ of adsorbing HCHO by doping TMs ascribed to the electron rearrangement and hybridization of Ce and TMs orbitals. The present work provides a beneficial guidance for exploring practical applications of the transition metal-doped $CeO_2$ as superior HCHO detection materials.

All the density functional theory calculations are carried out in the Vienna *Ab-initio* Simulation Package (VASP) [23], and VASPKIT [24] is used to post-process the data calculated by VASP. The generalized gradient approximation (GGA) is used with Perdew-Burke-Ernzerhof (PBE) [25,26] exchange- correlation functional. The Projector augmented-wave (PAW) method is used to deal with the core electrons, and the valence electrons are described by a plane wave basis set with a cutoff energy of 450 eV. The adsorption energy and electronic properties are calculated by *k*-point grid ($1 \times 1 \times 1$) and ($4 \times 4 \times 1$) Monkhorst-Pack grids, respectively. In order to avoid the interaction between periodic structures, the vacuum layer is set to 15 Å, and the convergence criteria of force and energy are set to 0.03 eV/Å and $10^{-5}$ eV, respectively.

The adsorption energy ($E_{ads}$) of HCHO adsorbed on $CeO_2$ surface that measures the strength of the interaction between HCHO and the surface, is calculated as

$$E_{ads} = E_{total} - E_{substrate} - E_{HCHO} \quad (1)$$

where $E_{total}$, $E_{substrate}$ and $E_{HCHO}$ represent the total energy of $CeO_2$ adsorbing HCHO, the energy of $CeO_2$ substrate and the energy of HCHO molecules in vacuum, respectively. It is be considered adsorption energies below −0.5 eV to be 'strong', or chemisorbed, while adsorption energies above −0.5 eV to be 'weak', or physisorbed in this work [27].

**Table 1**
C–O bond length of HCHO adsorbed on $\alpha$-$CeO_2$ and $\beta$-$CeO_2$ surfaces.

| Facets | Adsorption site | | |
|---|---|---|---|
| | Top | Bridge | Hollow |
| $\alpha$-$CeO_2$(100) | 1.30233 | 1.33086 | 1.43549 |
| $\alpha$-$CeO_2$(110) | 1.21506 | 1.22334 | 1.43392 |
| $\alpha$-$CeO_2$(111) | 1.25446 | 1.42322 | 1.41049 |
| $\beta$-$CeO_2$(100) | 1.43502 | 1.42711 | 1.42614 |
| $\beta$-$CeO_2$(110) | 1.29739 | 1.32099 | 1.32985 |
| $\beta$-$CeO_2$(111) | 1.21724 | 1.23043 | 1.22616 |

The binding energy ($E_{binding}$) of TMs doped $CeO_2$ is calculated as follows:

$$E_{binding} = E_{total} - E_{total-TM} - E_{TM} \quad (2)$$

Among them, $E_{total}$, $E_{total\text{-}TM}$ and $E_{TM}$ represent the energy of TM doped $CeO_2$, the energy of TM doped $CeO_2$ without TM, and the energy of a metal atom in vacuum, respectively. The negative value of $E_{bindin}$ indicates that the doping of TM is an exothermic reaction. In general, the more negative their values are, the more stable the adsorption is.

In order to simulate the sensitivity of selected TM-$\alpha$-$CeO_2$(100) (TM = Au, Hf, Nb, Ta, Zr), characteristics between sensor response and the current-voltage are calculated based on the nonequilibrium Green's function formalism of the SMEAGOL package [28]. The double-zeta basis with a cut off energy of 600 Ry and generalized gradient approximation of Perdew−Burke−Ernzerhof were used. The Brillouin zone is set on $1 \times 8 \times 10$ and $1 \times 10 \times 10$ Monkhorst-Pack *k*-meshes in the electrode and transport calculations, respectively.

Two $CeO_2$ phases, noted as $\alpha$-$CeO_2$ and $\beta$-$CeO_2$, are employed to simulate. As shown in Fig. S1a (Supporting information), $\alpha$-$CeO_2$ in a cubic fluorite structure with the space grouping $Fm\bar{3}m$ [29]. Ce is surrounded by eight nearby O, while O is surrounded by four nearby Ce. The lattice parameters are $a = b = c = 5.411$ Å, $\alpha = \beta = \gamma = 90°$ As shown in Fig. S1b (Supporting information, $\beta$-$CeO_2$ with the space group is $P4_2/mnm$ and the lattice constant is $a = b = 5.135$ Å, $c = 3.636$ Å, $\alpha = \beta = \gamma = 90°$ in order to compare with $\alpha$-$CeO_2$. The low index surfaces of $CeO_2$ are $CeO_2$(100), $CeO_2$(110) and $CeO_2$(111) [30,31]. The surfaces of $\alpha$-$CeO_2$ and $\beta$-$CeO_2$ before and after optimization are demonstrated in Figs. S1c-f (Supporting information) and Figs. S1g-l (Supporting information), respectively. According to previous report, the most favorable configuration for HCHO adsorption over stoichiometric oxides is normal to the surface with the oxygen bound to the metal cation [32]. The three sites (top, bridge and hollow) of HCHO adsorbed vertically on $\alpha$-$CeO_2$ and $\beta$-$CeO_2$ surfaces above Ce atom are selected in Fig. S2 (Supporting information).

After structural optimization, eighteen stable models are obtained. The adsorption energies and C–O bond length (*d*) of HCHO are used to evaluate the adsorption stability of HCHO on three facets. As describe in Table 1 and Figs. 1a and b, the lowest adsorption energies of HCHO on $\alpha$-$CeO_2$(100), $\alpha$-$CeO_2$(110), $\alpha$-$CeO_2$(111), $\beta$-$CeO_2$(100), $\beta$-$CeO_2$(110), $\beta$-$CeO_2$(111) are −2.99 eV, −1.49 eV, −1.56 eV, −3.67 eV, −1.50 eV and −1.35 eV, respectively. It is considered that adsorption energies below −0.5 eV is to be 'strong', or chemisorbed [27]. All of them are lower than −0.5 eV, indicating that the adsorption of HCHO on $CeO_2$ belongs to chemical adsorption. It is worth noting that their corresponding bond lengths are longer than the other two adsorption sites. For instance, adsorption energies of $\alpha$-$CeO_2$(100) on three sites are hollow (−2.99 eV) > bridge (−1.51 eV) > top (−1.12 eV). Their corresponding C–O bond length are hollow (1.44 Å) > bridge (1.33 Å) > top (1.30 Å). The more negative adsorption energy and the longer bond distance with interacting of $CeO_2$ surfaces and HCHO indi-

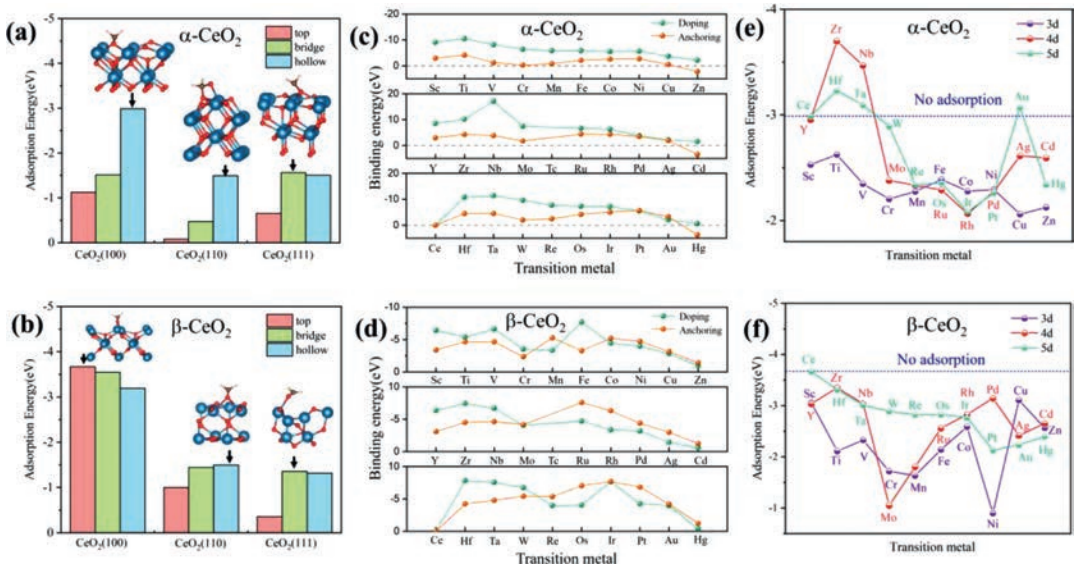


**Fig. 1.** Adsorption energies of HCHO at three adsorption sites (top, bridge and hollow) of (a) $\alpha$-$CeO_2$ and (b) $\beta$-$CeO_2$. Binding energies of TM doping at two sites of (c) $\alpha$-$CeO_2$(100) and (d) $\beta$-$CeO_2$(100). Yellow and green spots indicate that TMs are doped on anchoring site and doping site, respectively. Adsorption energies of HCHO adsorbed by (e) TM-$\alpha$-$CeO_2$ and (f) TM-$\beta$-$CeO_2$ (TM = Sc, Ti, V, Cr, Mn, Fe, Co, Ni, Cu, Zn, Y, Zr, Nb, Mo, Ru, Rh, Pd, Ag, Cd, Hf, Ta, W, Re, Os, Ir, Pt, Au, Hg).

cate higher performance to adsorb HCHO. Therefore, the orders of adsorption capacity of HCHO on $CeO_2$ are $\alpha$-$CeO_2$(100) > $\alpha$-$CeO_2$(111) > $\alpha$-$CeO_2$(110) and $\beta$-$CeO_2$(100) > $\beta$-$CeO_2$(110) > $\beta$-$CeO_2$(111). The hollow site for HCHO of $\alpha$-$CeO_2$(100) and the top site for HCHO of $\beta$-$CeO_2$(100) are employed in the following simulation.

In order to explore the favorable adsorption sites to TMs doping on $CeO_2$, 28 candidate TMs (TM = Sc, Ti, V, Cr, Mn, Fe, Co, Ni, Cu, Zn, Y, Zr, Nb, Mo, Ru, Rh, Pd, Ag, Cd, Hf, Ta, W, Re, Os, Ir, Pt, Au, Hg) are designed to investigate their binding energies at anchoring site and doping site of $CeO_2$. The structural models are displayd in Fig. S3 (Supporting information). According to the comparison of binding energies (Figs. 1c and d), it is show that (i) for TM-$\alpha$-$CeO_2$(100), most of TMs are apt to be doped at the doping site, while Pt and Au are more squint towards be doped at the anchoring site. For TM-$\beta$-$CeO_2$(100), TMs before the VIB group of the elements periodic table are apt to be adsorbed at the doping site. However, the TMs after the VIIB group of the elements periodic table are more inclined to be adsorbed at the anchoring site (except Fe); (ii) TMs doping is an exothermic reaction in virtue of their binding energies below 0 eV (except for IIB group TMs since they with no incomplete d shell and their electronic properties are not active). In the following simulation, doping site for TM-$\alpha$-$CeO_2$(100) is employed to adsorb HCHO. As for TM-$\beta$-$CeO_2$(100), we use sites that TMs are more inclined to doping.

To explore the adsorption capacity of TM doped $\alpha$-$CeO_2$(100) and $\beta$-$CeO_2$(100) to with HCHO, their adsorption energies and electronic properties are calculated. The calculated results of adsorption energies are displayed in Figs. 1e and f. Among them, the adsorption energies of five TM doped $\alpha$-$CeO_2$(100) are lower than $\alpha$-$CeO_2$(100). They are Zr-$\alpha$-$CeO_2$ (−3.70 eV), Nb-$\alpha$-$CeO_2$ (−3.47 eV), Hf-$\alpha$-$CeO_2$ (−3.23 eV), Ta-$\alpha$-$CeO_2$ (−3.09 eV) and Au-$\alpha$-$CeO_2$ (−3.07 eV), respectively. It indicates that the adsorption capacity of $CeO_2$ for HCHO is slightly enhanced owing to five TMs doped. However, the adsorption energies of TM doped $\beta$-$CeO_2$(100) are higher than $\beta$-$CeO_2$(100), indicating that $\alpha$-$CeO_2$(100) is more suitable for adsorbing HCHO. The transition states and the structural parameters of HCHO adsorb at TM-$\alpha$-$CeO_2$(100) (TM = Au, Hf, Nb, Ta, Zr) are displayed in Figs. S4 and S5 (Supporting information), respectively. The *d*(Ce-O) and A(H–C-H) of TM-$\alpha$-$CeO_2$(100) are smaller than $\alpha$-$CeO_2$(100). It is consistent with the result of adsorption energies.

Partial density of states (PDOS) and d-band center are used to further explain the mechanism that TM doped $\alpha$-$CeO_2$(100) increases the $CeO_2$ adsorption capacity of HCHO. As shown in Fig. 2a, the d orbitals of TMs and the d orbitals of Ce hybridized obviously from −6 eV to −4 eV. The d orbitals of Ce have obviously changed indicating that TM doped changes the d orbit of Ce, rearranges the electrons of the Ce, result in TMs can be stably doped on the surface of $CeO_2$. According to above results, it is concluded that the adsorption performance of HCHO on $\alpha$-$CeO_2$(100) is stronger than HCHO on $\beta$-$CeO_2$(100).

The d-band center of Ce is calculated using the following method (Eq. 3):

$$\varepsilon_d = \frac{\int_{-\infty}^{\infty} n_d(\varepsilon)\varepsilon d\varepsilon}{\int_{-\infty}^{\infty} n_d(\varepsilon) d\varepsilon} \quad (3)$$

In general, the shift of d-band center away from the Fermi level will increase the filling of the antibond state, thus weakening the adsorption of the adsorbent, otherwise it will enhance the adsorption of the adsorbent [33]. In our results, the d-band of TM-$\alpha$-$CeO_2$(100) (TM = Au, Hf, Nb, Ta, Zr) are closer to the Fermi level than $\alpha$-$CeO_2$(100), illustrating that TM doped increases the bonding state and led to the enhancement of the interaction between Ce and HCHO. Similarly, we find that the fermi level of HCHO adsorbed TM-$\alpha$-$CeO_2$(100) (TM = Au, Hf, Nb, Ta, Zr) have a red shift (Fig. 2b). Therefore, TM doped decreases the free energy of $\alpha$-$CeO_2$(100), resulting in more stable structure [34].

The Charge density difference (CDD) is employed to further clarify the electron transfer mechanism of HCHO adsorbed on TM-$\alpha$-$CeO_2$(100), it is calculated by Eq. 4.

$$\rho = \rho_{TM-CeO_2-HCHO} - \rho_{TM-CeO_2} - \rho_{HCHO} \quad (4)$$

In the formula, $\rho_{TM\text{-}CeO2\text{-}HCHO}$, $\rho_{TM\text{-}CeO2}$ and $\rho_{HCHO}$ are the charge densities of HCHO adsorbed on TM-$\alpha$-$CeO_2$(100), $\alpha$-$CeO_2$(100) and isolated HCHO molecule, respectively. As displayed in Fig. 2c, the yellow and cyan areas denote the charge accumulation and loss, respectively. It reveals that the C atom of HCHO obtains electrons from two Ce atoms of $\alpha$-$CeO_2$(100). After doping TM, the C atom with HCHO is inclined to obtain electrons from TM

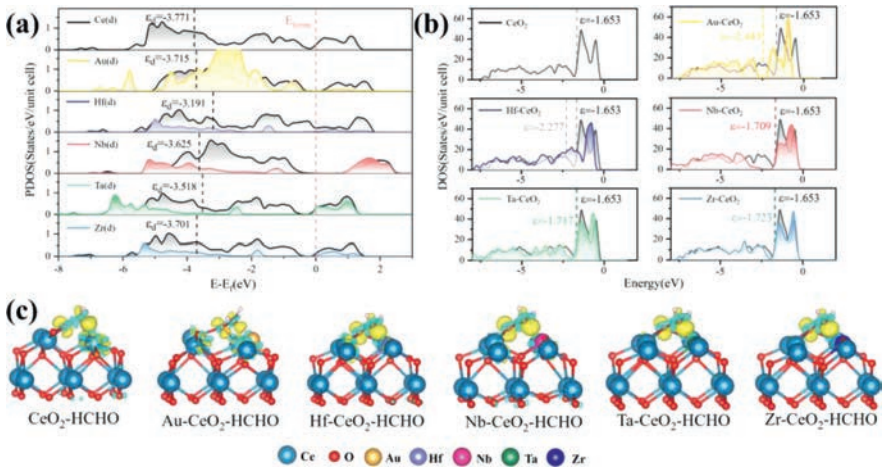


**Fig. 2.** (a) PDOS of HCHO adsorb at TM-$\alpha$-$CeO_2$(100) (TM = Au, Hf, Nb, Ta, Zr). 0 eV represents Fermi level. The black lines represent the D-band of Ce in HCHO adsorb at TM-$\alpha$-$CeO_2$(100) (TM = Au, Hf, Nb, Ta, Zr). (b) The DOS of HCHO adsorb at TM-$\alpha$-$CeO_2$(100) (TM = Au, Hf, Nb, Ta, Zr). (c) The charge density difference of TM-$\alpha$-$CeO_2$(100) (TM = Au, Hf, Nb, Ta, Zr).

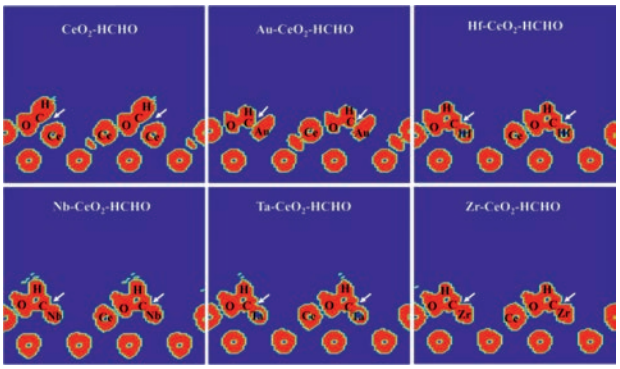


**Fig. 3.** Electron localization function of HCHO adsorb at TM-$\alpha$-$CeO_2$(100) (TM = Au, Hf, Nb, Ta, Zr). The white arrow points to the adsorption site of $CeO_2$ surface and HCHO, and the connection of TMs to HCHO indicates strong adsorption capacity. The saturation value is 0.1.

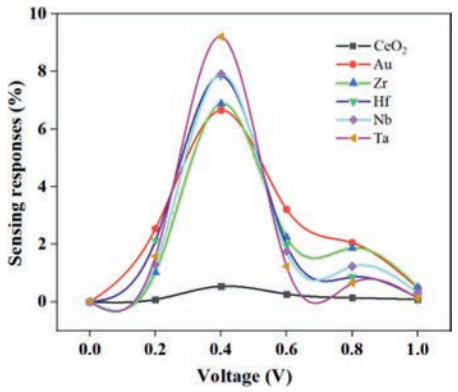


**Fig. 4.** Current–voltage characteristics along the TM-$\alpha$-$CeO_2$(100) (TM = Au, Hf, Nb, Ta, Zr) directions for sensing responses of HCOH.

result in forming covalent bonds of C of TM. Additionally, electron localization function (ELF) maps confirm that HCHO has a strong bonding with TM-$\alpha$-$CeO_2$(100) (TM = Au, Hf, Nb, Ta, Zr) but a weak interaction with $\alpha$-$CeO_2$(100) (Fig. 3). Hence, the TM doped promote the adsorption of HCHO on TM-$\alpha$-$CeO_2$(100).

Fig. 4 shows the current–voltage characteristics along the TM-$\alpha$-$CeO_2$(100) (TM = Au, Hf, Nb, Ta, Zr) after the adsorption of a HCHO molecule. When a voltage of 0.4 V is applied, the sensing response is the highest for HCHO for all of transport directions. As an applied voltage increases, the sensing response follows the order, Au >> Zr > Nb > Hf > Ta > substrate. Therefore, at an applied voltage of 0.4 V, it is concluded that Au-$\alpha$-$CeO_2$(100) shows excellent sensitivity performance than other TM-$\alpha$-$CeO_2$(100) sensor.

In conclusion, we proposed two $CeO_2$ phases ($Fm\bar{3}m$ and $P4_2/mnm$), three facets ($CeO_2$(100), $CeO_2$(110) and $CeO_2$(111)) and three adsorption sites (top, bridge and hollow) as substrate models. DFT calculation reveals that (i) The hollow site for HCHO of $\alpha$-$CeO_2$(100) and the top site for HCHO of $\beta$-$CeO_2$(100) are considered to be suitable for the adsorption of HCHO by comparing adsorption energies; (ii) TM-$\alpha$-$CeO_2$(100) (TM = Au, Hf, Nb, Ta, Zr) are screened as candidate materials to absorb HCHO on account of TM doped improves the performance of adsorbing HCHO; (iii) TM doped changes the d orbit, rearranges the electrons of Ce, causes $\alpha$-$CeO_2$(100) with lower free energy result in TM doped improves the performance of $\alpha$-$CeO_2$(100) for adsorbing HCHO; (iv) C atom gets electrons and forms covalent bond with TM contribute to improve the performance of surfaces for adsorbing HCHO. These findings would provide a route to design HCHO sensor materials with superior performance.

## Declaration of competing interest

We declare that we have no financial and personal relationships with other people or organizations that can inappropriately influence our work, there is no professional or other personal interest of any nature or kind in any product, service and/or company that could be construed as influencing the position presented in, or the review of, the manuscript entitled.

## Acknowledgments

This work was supported by the National Natural Science Foundation of China (No. 22005269); the NSFC-Zhejiang Joint Fund for Integration of Industrialization and Diversification (No. U1809214); the National Natural Science Foundation of Zhejiang Province (No. LQ21B030007) and the Science and Technological program of Ningbo (No. 2021S136)

## Supplementary materials

Supplementary material associated with this article can be found, in the online version, at doi:10.1016/j.cclet.2022.04.074.

## References


[1] T. Salthammer, S. Mentese, R. Marutzky, Chem. Rev. 110 (2010) 2536–2572.
[2] J. Mo, Y. Zhang, Q. Xu, J.J. Lamson, R. Zhao, Atmos. Environ. 43 (2009) 2229–2246.
[3] A. Casset, C. Marchand, A. Purohit, et al., Allergy 61 (2006) 1344–1350.
[4] X. Tang, Y. Bai, A. Duong, et al., Environ. Res. 35 (2009) 1210–1224.
[5] T. Salthammer, Angew. Chem. Int. Ed. 52 (2013) 3320–3327.
[6] P. Chung, C. Tzeng, M. Ke, C. Lee, Sensors 13 (2013) 4468–4484.
[7] C. Gong, W. Huang, J. Liu, et al., Fuel 221 (2018) 188–195.
[8] D. Yuan, L. Tian, D. Gu, et al., J. Cleaner Prod. 156 (2017) 310–316.
[9] X. Cui, G. Fang, L. Jiang, S. Wang, Anal. Chim. Acta 590 (2007) 253–259.
[10] A. Allouch, M. Guglielmino, P. Bernhardt, C.A. Serra, S. Le Calvé, Sens. Actuators B 181 (2013) 551–558.
[11] Y.J. Jeong, W. Koo, J. Jang, et al., Nanoscale 10 (2018) 13713–13721.
[12] J. Kang, J. Jang, W. Koo, et al., J. Mater. Chem. A 6 (2018) 10543–10551.
[13] Q. Chen, C. Yuan, C. Zhai, Chin. Chem. Lett. 33 (2022) 983–986.
[14] B. Bai, Q. Qiao, J. Li, J. Hao, Chin. J. Catal. 37 (2016) 102–122.
[15] Y. Abghoui, E. Skúlason, J. Phys. Chem. B 121 (2017) 24036–24045.
[16] S. Hussain, N. Aslam, X.Y. Yang, et al., Ceram. Int. 44 (2018) 19624–19630.
[17] P. Zhang, L. Zhang, H. Xu, et al., Rare Met. 40 (2021) 1614–1621.
[18] D.S. Daniel, S. Ernest, S. Fairose, Mater. Today Proc. 38 (2021) 3332–3336.
[19] R.G. Parr, S.R. Gadre, L.J. Bartolotti, Proc. Natl. Acad. Sci. U. S. A. 76 (1989) 2522–2526.
[20] X. Deng, X. Liang, S. Ng, C.L. Wu, Appl. Surf. Sci. 484 (2019) 1244–1252.
[21] J. Hu, C. Zhai, M. Zhu, Chin. Chem. Lett. 32 (2021) 1348–1358.
[22] M. Jing, W. Song, L. Chen, et al., Faraday Discuss. R. Soc. Chem. 122 (2018) 438–448.
[23] G. Kresse, J. Furthmüller, Phys. Rev. B 54 (1996) 11169–11186.
[24] V. Wang, N. Xu, J. Liu, G. Tang, W. Geng, Comput. Phys. Commun. 267 (2021) 108033.
[25] J.P. Perdew, K. Burke, M. Ernzerhof, Phys. Rev. Lett. 77 (1996) 3865–3868.
[26] J.P. Perdew, K. Burke, M. Ernzerhof, Phys. Rev. Lett. 78 (1997) 1396–5001.
[27] D. Mei, N. Aaron Deskins, M. Dupuis, Surf. Sci. 601 (2007) 4993–5001.
[28] I. Rungger, S. Sanvito, Phys. Rev. B 78 (2008) 035407.
[29] Y. Zhang, S. Zhao, J. Feng, et al., Chem 7 (2021) 2022–2059.
[30] Y. Lin, Z. Wu, J. Wen, K.R. Poeppelmeier, L.D. Marks, Nano Lett. 14 (2014) 191–196.
[31] Y. Li, W. Shen, Chem. Soc. Rev. 43 (2014) 1543–1574.
[32] H. Liu, X. Wang, C. Pan, K.M. Liew, J. Phys. Chem. C 116 (2012) 8044–8053.
[33] Z. Chen, Y. Song, J. Cai, et al., Angew. Chem. Int. Ed. 57 (2018) 5076–5080.
[34] F. CalleVallejo, D. Loffreda, M.T.M. Koper, P. Sautet, Nat. Chem. 7 (2015) 403–410.